EES Batteries

Accepted Manuscript

This article can be cited before page numbers have been issued, to do this please use: S. Lin, W. Li, H. Yang, M. Chen, H. Xie, Y. Qin, J. Zeng, P. Zhang and J. Zhao, *EES Batteries*, 2025, DOI: 10.1039/D5EB00077G.

View Article Online
DOI: 10.1039/D5EB00077G

Broader context

Due to the advantages of abundant resources, controllable cost and excellent safety, sodium-ion batteries (SIBs) have become a supplement for lithium-ion batteries. The SIBs utilizing a $NaNi_{1/3}Fe_{1/3}Mn_{1/3}O_2$ (NFM) cathode paired with hard carbon (HC) anode exhibit relatively high energy density, thus demonstrate promising application prospects in large-scale energy storage systems. And elevating the charging cutoff voltage offers a more universally applicable strategy to further enhance energy density compared with the material approaches. However, the accelerated degradation mechanisms induced by high-voltage operation severely compromise cycle life, creating a critical barrier to commercialization. A systematic evaluation and comprehensive understanding of high-voltage degradation mechanism of NFM//HC batteries is the foundation for the development of long cycle life with high energy density for SIBs. In this study, the cycling performance and degradation mechanism/source under different upper voltages are explored, and the degradation boundary between normal and abuse working conditions of battery is clarified. The degradation source quantified by reverse coin half-battery is mainly from active Na^+ loss, while the active NFM loss is significantly aggravated at 4.2 V due to an irreversible X and O3' phase transition. Finally, a powerful case strategy of electrolytes with boron-contained additives shows enhanced all-round performance of NFM cathode for high capacity with long cycling life.

View Article Online
DOI: 10.1039/D5EB00077G

ARTICLE

High-voltage Cycling Degradation Mechanisms of $NaNi_{1/3}Fe_{1/3}Mn_{1/3}O_2$ Cathode in Sodium-Ion Pouch Cells

Received 00th January 20xx,
Accepted 00th January 20xx

DOI: 10.1039/x0xx00000x

Shini Lin [a], Wei Li [a], Huiya Yang [a],Minghui Chen [a], Honghao Xie [a], Yuan Qin [a], Jing Zeng *[a], Peng Zhang *[b] and Jinbao Zhao *[a]

Sodium-ion batteries (SIBs) utilizing $NaNi_{1/3}Fe_{1/3}Mn_{1/3}O_2$ (NFM) cathode paired with hard carbon (HC) anode exihibit relatively high energy density. To further enhance energy density, elevating the charging cutoff voltage offers a more universally applicable strategy, compared with the material approaches which may encounter limitations due to raw material cost and supply constraints. However, the accelerated degradation mechanisms induced by high-voltage operation severely compromise cycle life, creating a critical barrier to commercialization. This work reveals the high-voltage degradation mechanism of NFM cathode at the full battery level, from evaluating electrochemical performance with upper voltage to profiling the structural characterization and evolution, interfacial reactions tracking, reaction kinetics analysis, and transition metal dissolution quantification. The HC||NFM battery cycling at 4.2 V charging cut-off voltage has significantly reduced capacity retention rate (55%, 300 cycles) due to the interfacial side reactions and NFM structure degradation, though it has much higher initial capacity. The cathode undergoes an irreversible structural evolution (X and O3' phases) with frequent cell volume expansion/contraction exacerbating particle cracking and interfacial parasitic reactions. While that at 4.0 V upper voltage maintains a good balance between high capacity and long cycle life due to the simple reversible structural evolution of NFM (O3-P3-O3) and the moderate impedance during cycling. Finally, electrolyte with boron-contained additives were demonstrated as an effective strategy to improve the comprehensive performance of NFM at high voltage. The mechanistic insights and material modification strategy presented herein pave the way for engineering high-performance layered oxide cathodes that concurrently achieve extended cyclability and high energy density in SIBs.

Introduction

In recent years, sodium-ion batteries (SIBs) have become a supplementary energy-storage technology coping with the resource scarcity dilemma and restraining the inordinate price fluctuation of lithium-ion batteries (LIBs), highlighting its abundant crustal-marine resources, affordable cost, excellent battery performances, and compatible manufacturing craft with LIBs. [1–5] However, its energy density is unsatisfactory, limiting its further application. Thus, the growing demand for higher energy density of SIBs will be a future mainstream trend through materials selection and optimization, battery manufacturing technology, and pack structure design. [6–9]

The mature layered transition metal oxide, $NaNi_{1/3}Fe_{1/3}Mn_{1/3}O_2$ (NFM), has become one of the most promising cathode materials through long-term researches, due to its high capacity, high voltage, environmental friendliness and easy production. [10–12] Hard carbon (HC), also characterizing high capacity, low voltage plateau and extensive-source raw materials, presents brilliant prospects as the anode. [13–18] Consequently, the HC||NFM battery has relatively high energy density among SIBs and can be a typical model case to be further researched and developed. However, poor cycling stability attaches to this electrochemical system, curtailing its practical application lifespan. This weakness to a great extent is imputed to the instability of NFM cathode. [19] In the practical application scenarios, in order to achieve the higher energy density goal, the increased charging cut-off voltage can be a highly-universal strategy. [20] Elevating the charge cutoff voltage facilitates enhanced Na^+ deintercalation from the layered cathode framework, enabling greater active ion participation in redox reactions and thereby achieving concurrent improvements in both operating voltage and reversible capacity. But as a trade-off, the cycling stability weakness will be further magnified because the higher cut-off voltage poses a greater challenge to the structure stability of cathode. [11,21] The cathode experiences a severer phenomenon of crystal phase evolution, particle cracking, side reactions at the interface with the electrolyte, and transition metal (TM) dissolution.

The multidimensional method for improving the cycling stability of NFM cathode under normal conditions or high charging cut-off voltages has been widely researched. For example, doping and mixed phase design inhibit the harmful

[a] State-Province Joint Engineering Laboratory of Power Source Technology for New Energy Vehicle, State Key Laboratory of Physical Chemistry of Solid Surfaces, Engineering Research Center of Electrochemical Technology, Collaborative Innovation Center of Chemistry for Energy Materials, College of Chemistry and Chemical Engineering, Ministry of Education, Xiamen University, Xiamen 361005, China
[b] College of Energy & School of Energy Research, Xiamen University, Xiamen 361102, China
†Electronic supplementary information (ESI) available. See
DOI: 10.1039/x0xx00000x

O3'/OP2 phase transition, surface coating and electrolyte modification enhance the interface stability under high voltages. [22–28] However, most of the work are only focused on the material level and have no prolongation to the battery level or actual working condition. Due to the potential difference between Na metal anode and HC anode during charge/discharge cycling and the unique sodium storage mechanism of HC, the degradation mechanism of NFM cathode on material level (Na||NFM) and battery level (HC||NFM) cannot be bracketed. Additionally, there are few reports on elucidating the structural evolution process of NFM in pouch battery or dissecting the cycling failure mechanism combined with different charging cut-off voltages. Limitedly, the coin battery system has been taken as the main research object so far, which has a certain gap with the battery architectures for practical industrialization. Therefore, relevant research based on HC||NFM pouch batteries is helpful to analyze the battery performance failure process dominant by the NFM cathode on the premise of fitting actual working condition, so as to provide a feasible scheme for the cathode modification and battery application.

In this work, HC||NFM pouch battery was assembled to systematically analyze the high-voltage failure mechanism. On battery level, combined with reverse coin half battery, the detailed degradation mechanism of HC||NFM battery was quantitatively analyzed. The structural evolution of NFM cathode in pouch battery was for the first time non-destructively traced by operando XRD, with the original battery architecture. The HC||NFM batteries during cycling at different charging cut-off voltages were dissembled for the postmortem analysis of phase transition, particle crack, interface thickening, and TM dissolution/migration/deposition. At 4.0 V cut-off voltage, the HC||NFM battery holds both the high energy density and the long cycle stability (capacity retention=73% after 300 cycles). This benefits from the simple reversible O3-P3-O3 structural evolution of NFM cathode per cycle. In contrast, at 4.2 V cut-off voltage, the HC||NFM battery shows large capacity fading (capacity retention=55% after 300 cycles) and severe voltage attenuation despite the high energy density at initial 100 cycles. Reverse coin half battery tests tell that it results from the interfacial side reactions (impedance: NFM>HC) and cathode structural degradation. During one cycle, NFM undergoes a complex and irreversible O3-P3-X-O3'-P3-O3 structural evolution, with frequent unit cell volume expansion and contraction, resulting in the structural instability (phase transition presented in the ex-situ XRD and 32 mAh/g capacity loss). While NFM at 4.0 V and 3.8 V upper voltages has the unit cell volume expansion and contraction only once during one cycle. Thus, NFM at 4.2 V upper voltage has earlier particle cracking and severer side reactions with the electrolyte. Through ICP tests, Fe and Mn have significant dissolution in the electrolyte from NFM. Finally, a case of improvement strategy was provided as boron-contained electrolyte additives optimizing interface and showing excellent performance. This work designates the high-voltage failure mechanism of HC||NFM batteries, laying the foundation of developing structure-stable high-voltage layered cathode and long-life high-specific-energy SIBs.

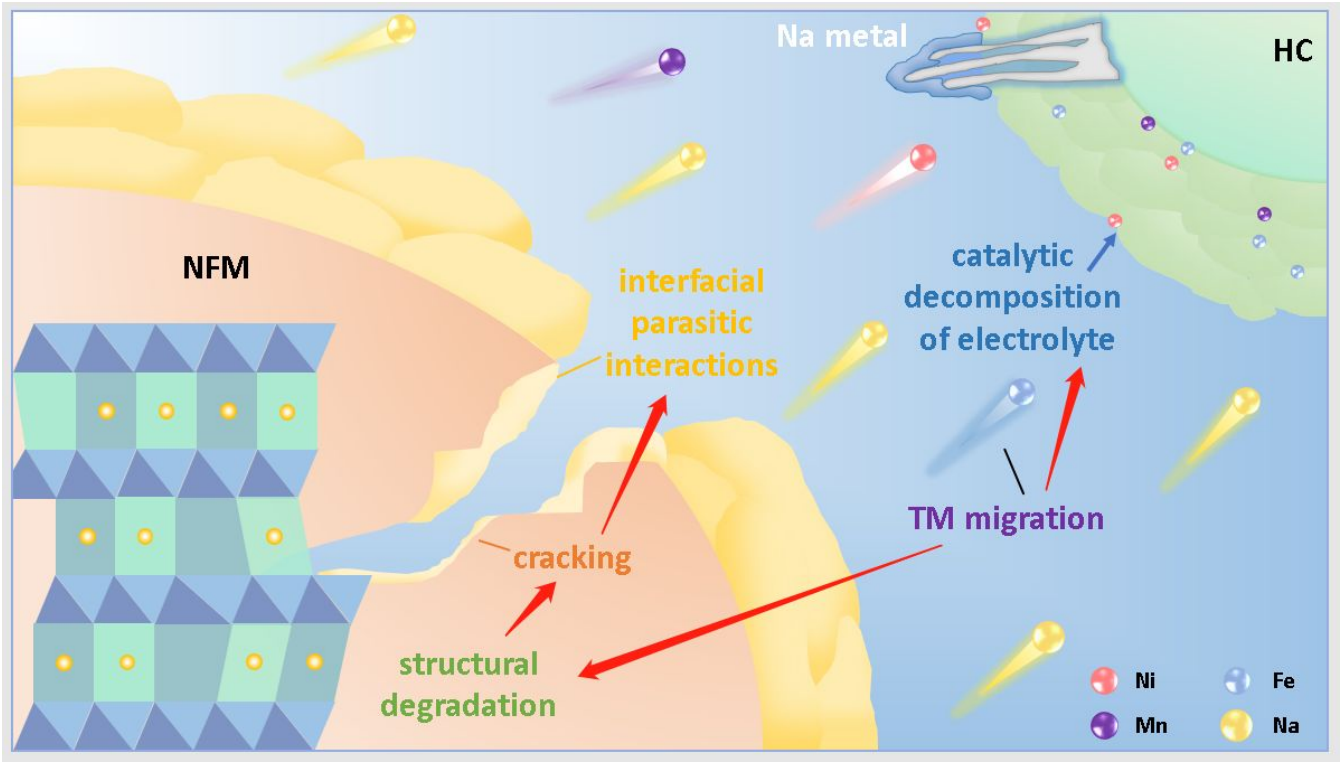

Scheme 1 General model of the degradation and chemical crosstalk of NFM cathode in practical sodium-ion full battery.

Results and discussion

1. Electrochemical degradation source

NFM has a $NaFeO_2$ structure with $R\bar{3}m$ space group, with the ion-diffusion controlled electrochemical reaction, and there is a large capacity increment of 27 mAh/g with the upper voltage increase from 4.0 V to 4.2 V (Fig. S1-17). At 4.0 V upper voltage, NFM shows both the high capacity and stable cycling (capacity retention=86%/81% after 300/500 cycles, Fig. S9). To benchmark commercial sodium-ion batteries, HC with promising applications was selected as the anode to analyze the degradation mechanism of NFM on battery level. [29] Also, the HC||NFM pouch battery has a large energy density increment of 26.7 Wh/kg with the charging cut-off voltage increase from 4.0 V to 4.2 V, illustrating the charging cut-off voltage increase is an effective way to improve the energy density of battery (Fig. S18a). Different from Na metal and other anode, HC has a unique sodium-ion storage mechanism of adsorption-intercalation-filling (Fig. S18b). The sodium ion loss on HC such as SEI formation and Na metal deposition, will cause less Na^+ back to the NFM cathode and more intense phase transition (Fig. S18c). Due to the voltage change of HC anode during cycling, the NFM cathode may have a different degradation process in full battery compared with half battery (Fig. S18d-f). Additionally, the voltage of NFM cathode in full battery examined by three-electrode pouch battery is quite different from that in half battery especially for the discharge process (Fig. S18g-i and S19). These reveal that evaluating the NFM failure with full battery is essential and beneficial to battery manufacturing optimization and material modification.

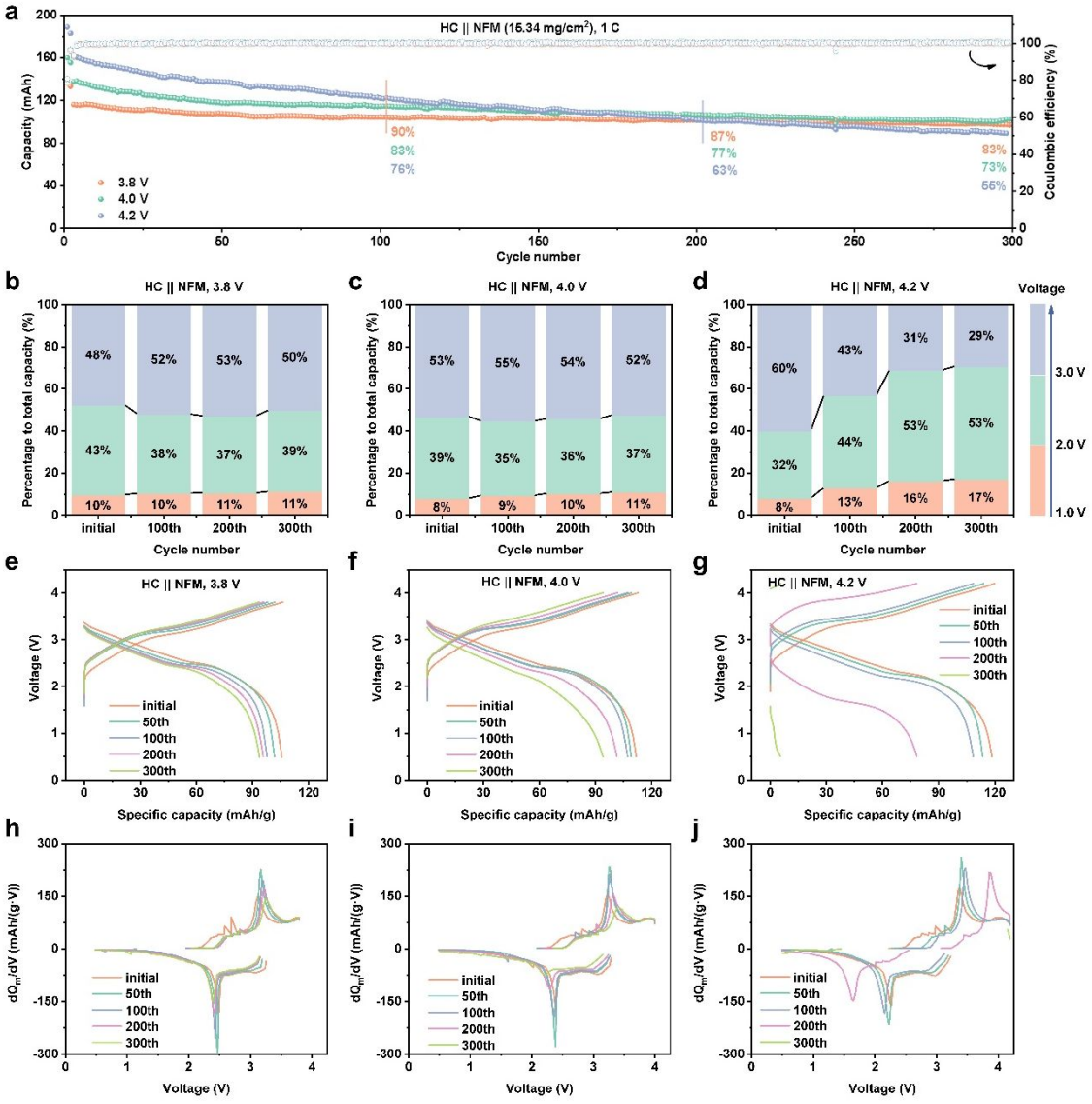

Fig. 1 (a) Cycling performance of HC||NFM pouch full battery with the upper voltages of 3.8 V, 4.0 V and 4.2 V. (b-d) Evolution of capacity distribution versus voltage of HC||NFM pouch full batteries cycling at the upper voltages of 3.8 V, 4.0 V, 4.2 V respectively. (e-g) Galvanostatic charge/discharge curves and (h-j) increment capacity curves of HC||NFM full battery cycling at the upper voltages of 3.8 V, 4.0 V, 4.2 V respectively.

View Article Online
DOI: 10.1039/D5EE00077G

Therefore, HC||NFM battery (information of HC anode was in Fig. S20-24) was assembled and relevant battery parameters are listed in Table S1. When the upper voltage increases from 4.0 V to 4.2 V, the capacity retention drops from 73% to 55% obviously, and the capacity decreases gradually throughout the 300 cycles, revealing the cycling instability at 4.2 V (Fig. 1a). In addition, with the cycling, more capacity distributes at a lower voltage range (<3 V), indicating the severe voltage attenuation, while the other two (3.8 V and 4.0 V) have little change (Fig. 1b-d). The capacity fading and voltage attenuation jointly make a sharp energy density decline at 4.2 V for HC||NFM battery despite its early-stage high energy density. In comparison, at 4.0 V upper voltage, the capacity fading is concentrated in the early cycle stage, and the capacity distribution versus voltage is almost unchanged. On the whole, the energy density through the whole cycling is relatively stable. Thus, the critical charging cut-off voltage balanced with long-life and high-energy density may be 4.0 V. The HC||NFM coin full battery was also auxiliarily assembled. Similarly, at 4.2 V upper voltage, the capacity fading and voltage attenuation are significant than the other two (Fig. 1e-g and S25-26). And it is noticeable that the capacity decay and polarization increment are small in early 100 cycles but steeply climb around 200 cycles. It is speculated that due to the much larger internal resistance and polarization of coin battery, there is sodium deposition or dendrite formation on the anode, resulting in large capacity loss. There is a distinct oxidation peak near 4.2 V in the dQ/dV curve corresponding to the voltage plateau near 4.2 V in the charge-discharge curve (Fig. 1g and 1j). At 3.8 V and 4.0 V upper voltages, the capacity decay and polarization increment are moderate, exhibiting superior and comparable cycling stability (Fig. 1e-f and S26). Notably, the voltage plateaus around 3.3 V (charge) and 2.5 V (discharge) contribute to the large specific-capacity ratio (Fig. 1h-i). Through EIS of cycled HC||NFM batteries, the battery impedance increases with the charging cut-off voltage increase, especially significant from 3.8 V to 4.0 V (Fig. S27).

Subsequently, the reverse coin battery was reassembled from cycled pouch battery to quantitate the capacity degradation sources of HC||NFM battery at 3.8 V, 4.0 V and 4.2 V upper voltages. Active Na^+ loss, active NFM material loss and active HC material loss are the three capacity degradation sources, which the first one usually results from the interfacial side reactions, the second is rooted in the cathode structure degradation, and the third is due to the anode structure degradation. During the first cycle of Na||NFM, the charge capacity is generally less than the discharge one, and the difference value is larger than that

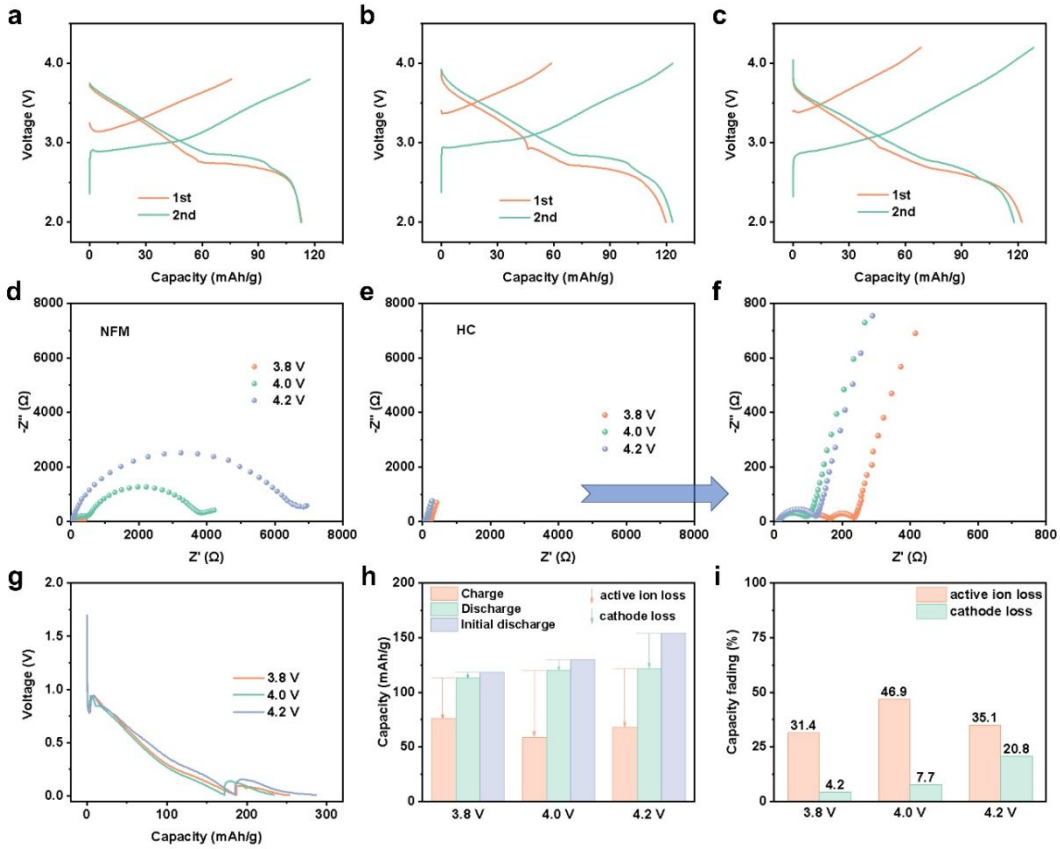

Fig. 2 Analysis of capacity degradation source. Charge/discharge curves of Na||NFM with the cathode from cycled pouch batteries at (a) 3.8 V, (b) 4.0 V and (c) 4.2 V upper voltages. EIS of (d) Na||NFM and (e-f) Na||HC, with the NFM and HC from cycled pouch batteries at 3.8 V, 4.0 V and 4.2 V upper voltages. (g) Discharge curves of HC anode from cycled pouch batteries at 3.8 V, 4.0 V and 4.2 V upper voltages. (h-i) Active Na^+ loss and active NFM loss to capacity fading.

View Article Online
DOI: 10.1039/D5EE00776C

between the initial discharge capacity and cycled discharge capacity, indicating the full battery capacity loss mainly from the active Na^+ loss (Fig. 2a-c, 2h-i). Besides, the charge/discharge capacity in the following cycle are similar to the discharge one in the first cycle, again proving the result of active Na^+ loss. Through EIS measurements, the impedance of NFM is significantly larger than that of HC, telling the ion diffusion difficulty in cathode (Fig. 2d-e). Besides, the charging cut-off voltage influences the impedance of NFM obviously, while it has no obvious effect on the impedance of HC (Fig. 2f). It is presumably related to the inequable oxidation reactions of the electrolyte on NFM at different upper voltages and the structure degradation of NFM. In the Na||HC reverse coin batteries, the initial discharge capacity almost has no decrease compared to that of fresh, illustrating the structural stability of HC anode in full battery (Fig. 2g). In the Na||NFM reverse coin batteries, the difference value between the fresh discharge capacity and the cycled discharge capacity represents the structural failure. And these exact values are 5 mAh/g (4.2%), 10 mAh/g (7.7%) and 32 mAh/g (20.8%) capacity loss for the cathode from cycled pouch batteries at 3.8 V, 4.0 V and 4.2 V respectively (Fig. 2h-i). The capacity loss at 4.2 V is significantly largest, indicating the severity of active NFM loss at high voltage.

2. Structural evolution of NFM in cycling pouch battery

The structural evolution of NFM in pouch battery was traced through operando XRD to explore the reasons for the surge in active cathode loss at high-voltage. Notably, the real-time non-destructive detection of NFM cathode was achieved in the original working environment (Fig. 3a). In the operando XRD results, the peaks of NFM cathode are stronger than those of other amorphous components in pouch battery and distinguished easily from those of Al foil (Fig. 3b-d). The structural evolution of NFM cathode for 3.8 V and 4.0 V upper voltages are similar as O3, P3, O3 phase transition sequence. In the initial 5-h charge stage, the NFM cathode experiences a solid-solution reaction of O3 phase with the expansion of c-axis and cell volume, indicated by the shift to a lower angle of (003) peak. The biphasic reaction is quick and not distinct in the subsequent desodiation process (full battery around 2.5 V). And in the reverse Na^+ intercalation process, the P3-O3 biphasic reaction also appears around 2.5 V of full battery. The (003) peak shift when full battery charges to 3.8 V and 4.0 V are almost equal, and it can be noticed that (003) peak of 4.0 V has a tendency to weaken and move to a higher angle, indicating the critical point from P3 to OP2 phase (Fig. 3e-f). While for the charge process of 4.2 V upper voltage, the (003) peak firstly shifts to a lower angle and then between 4.0-4.2 V in the reverse direction to a higher angle. Due to its reverse shift, the volume change of unit cell is severer than those of 3.8 V and 4.0 V upper voltages (Fig. 3d, 3g and Table S2). Besides, the XRD pattern when fully charged cannot be indexed to any known phase, characterizing the higher angle of (003) peak than the initial (shift=0.32°, Fig. 3g), the (006) peak vanishing, and both the (101) and (102) peaks shifting to higher angle and overlapping, called "X" phase. [30] In the reverse process of Na^+ intercalation in NFM cathode, a structural evolution sequence of X, O3', P3, O3 occurs in NFM, while the other two (3.8 V and 4.0 V) have neither X phase nor O3' phase. Specifically, when full battery discharges from 4.2 V to 3.5 V, X-phase solid-solution reaction and X-O3' biphasic reaction happen successively in NFM cathode, with (003) peak shift to a lower angle. From 3.5 V to 3.3 V, it is hexagonal O3'-phase solid-solution reaction, with the two significant overlapping peaks of (101) and (102), (107) and (108) peaks, and (105) peak shift to 15.6°. In conclusion, the irreversible structural evolution at 4.2 V upper voltage aggravates the accumulation of local stress in NFM particles and reducing the structure stability, which is largely attributed to the harmful X and O3' phases with sodium ion deficiency in NFM.

In general, though the cathode from pouch battery cycling at 4.2 V upper voltage releases more capacity in the early cycles, it is also accompanied with the more intense structural evolution, which results in severe structural degradation, cracking, interfacial side reactions and large capacity loss (active ion loss and active NFM loss > 20%).

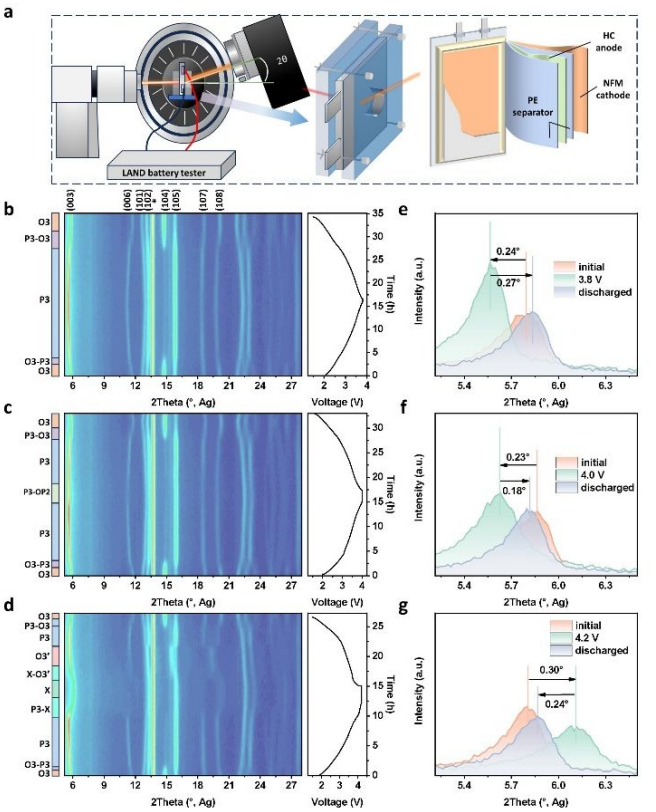

Fig. 3 Real-time structural evolution of NFM cathode in pouch batteries through non-destructive detection. (a) Schematic diagram of pouch-battery operando XRD measurements. (b-d) Operando XRD test results of NFM cathode in pouch battery cycling for 3.8 V, 4.0 V, and 4.2 V upper voltages respectively. (e-g) Local (003) peak shift at initial, fully charged, fully discharged states for 3.8 V, 4.0 V, and 4.2 V respectively.

3. Bulk structure-interface degradation

To deeply understand the electrochemical degradation mechanism of NFM material in full battery arising from its structural evolution as presented above, the NFM cathode was sampled at different cycles of high, normal and low charging cut-off voltage.

When cycling at 4.2 V upper voltage, the NFM cathode has an earlier phase transition as the vanished (104) peak at the 50th cycle, while those of 3.8 V and 4.0 V show better structure stability as (104) peak weakens slowly during cycle (Fig. 4a-c and S28-30). The (003) peak cycling at 3.8 V gradually shifts to a lower angle accompanied with unit cell volume

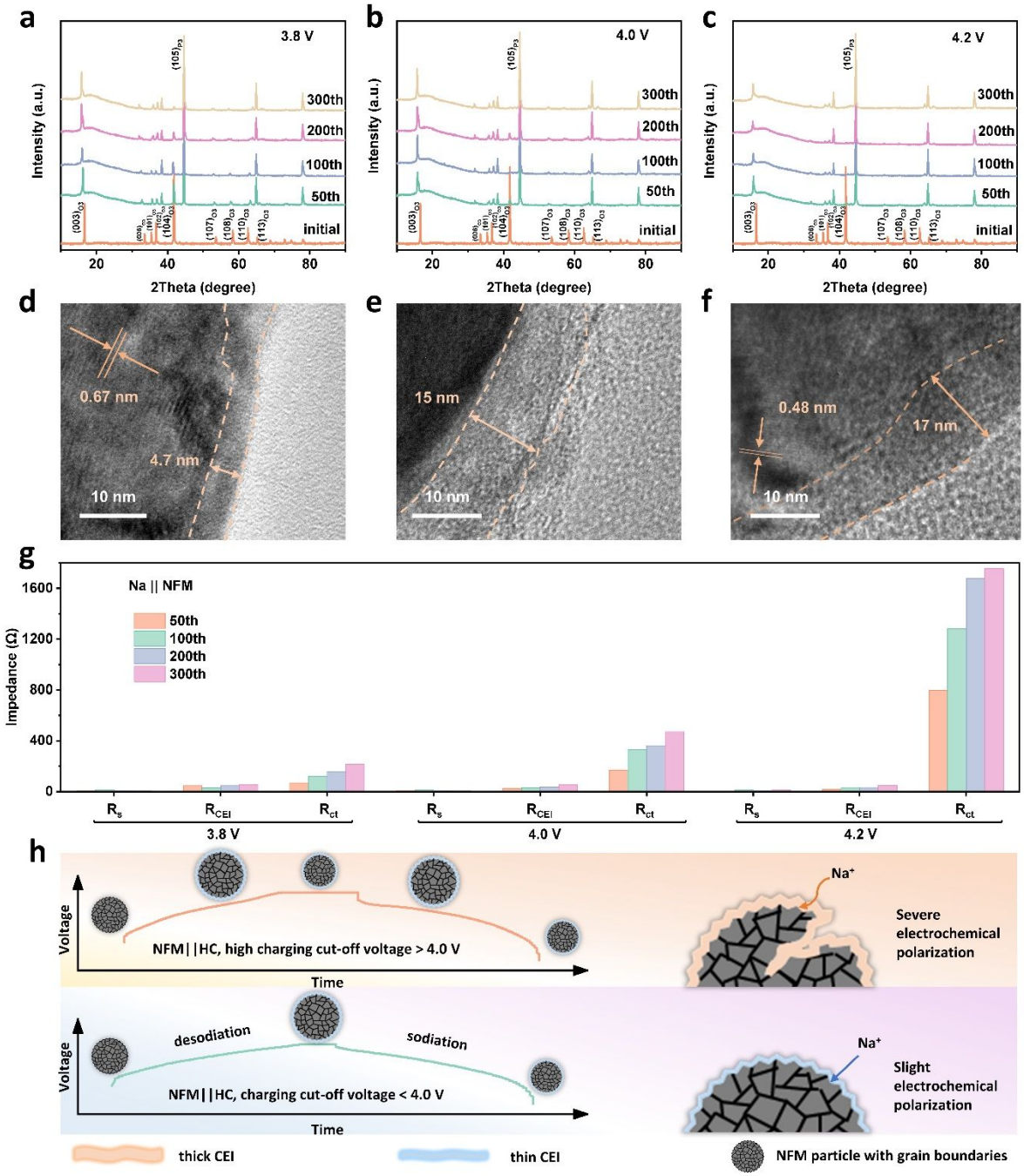

Fig. 4 Structure-interface evolution generating NFM cathode failure during cycling. (a-c) Postmortem XRD of NFM cathode from fully-discharged pouch batteries at different cycles of 3.8 V, 4.0 V and 4.2 V upper voltages. (d-f) TEM images of CEI of NFM from full-discharged pouch batteries after 300 cycles at 3.8 V, 4.0 V, and 4.2 V upper voltages respectively. (g) Fitted EIS data of fully-charged NFM cathode at different cycles of different upper voltages. (h) Failure mechanism of NFM cathode with cycling at high/normal voltages.

View Article Online
DOI: 10.1039/D5EB00077G

expansion, indicating the gentle structural degradation. While the (003) peak cycling at 4.0 V and 4.2 V have the significant shift in the first cycles, indicating structural degradation concentrating in the early cycling. Notably, the (104) peak near 42° indicating O3 phase in NFM cathode is accompanied with a peak near 16.2°, as can be seen in the cycled cathode of 3.8 V and 4.0 V upper voltages. While for 4.2 V, the (104) peak near 42° disappears, indicating the little O3 phase and significant structure transition of cathode. Thus, the concomitant peak near 16.2° will also disappear. Besides, from the operando XRD of 4.2 V upper voltage, during charge, the (006) peak shifts to low angle and disappears, the (101) and (102) peaks shift to high angle and only one peak leaves. Thus, the two characteristic (101) and (102) peaks between 35–37.5° in the cycled 4.2V sample nearly disappear, with the peak near 38° instead. The NFM cathode of 3.8 V upper voltage has obvious cracks in the 300th cycle, while that of 4.0 V is in the 200th cycle, and that of 4.2 V is in the 100th cycle, demonstrating frequent and intense phase transition causing particles to crack faster (Fig. S31). When particles crack, the continuing interfacial parasitic reactions between the exposed fresh surface and the electrolyte will make CEI thicker, affect the interfacial kinetics and lead to the loss of capacity (Fig. 4d-f). [31–34] Thus, the interfacial kinetics was traced through EIS. The fitted equivalent circuit model of EIS is in Fig. S32. The ion diffusion impedance of cathode/electrolyte interface (R_{CEI}) decreases with the charging cut-off voltage increase, indicating the interfacial components at high voltage more beneficial to ion diffusion (Fig. 4g, Fig. S33-35, and Table S3). While the R_{CEI} increases faster with the cycling at higher upper voltage, indicating the accelerated interfacial degradation at higher voltages. The charge transfer impedance (R_{ct}) is significantly larger than R_{CEI}, revealing that the electrochemical reaction of NFM cathode is a more obvious matter affecting battery performance than the ion diffusion in the interface. Additionally, R_{ct} increases significantly with the charging cut-off voltage increase, especially from 4.0 V to 4.2 V, indicating that the more sluggish electrode reactions at higher upper voltage. Thus, galvanostatic intermittent titration technique (GITT) was used to quantitatively evaluate the polarization evolution and Na^+ diffusion behavior changes in NFM material during cycling to predict the aging mechanism. The Na^+ diffusion coefficient (D_{Na^+}) increases from 3.0 V to 3.9 V ($\approx 2\times 10^{-9}$ cm^2/s), but decreases when the voltage continues to rise, well matching the R_{ct} change with the increased charging cut-off voltage in EIS results above (3.8 V < 4.0 V < 4.2 V) (Fig. S36). This further proves the sluggish electrochemical reaction kinetics above 4.0 V in the NFM cathode. Through polarization analysis in cycling for various upper voltages, the NFM desodiation/sodiation is proved to be mainly controlled by activation polarization (Fig. S37-38). Compared with 3.8 V upper voltage, the activation polarization of 4.0 V and 4.2 V upper voltages are significantly greater, and its increase with cycling is more serious. The systematic high-voltage failure mechanism of NFM cathode is shown in Fig. 4h.

4. TM dissolution in cathode

The irreversible migration of TM ions to Na^+ slabs in NFM cathode especially for high voltage will not only hinder the bulk-phase diffusion of active Na^+, but also dissolve, migrate driven by the anode potential, and deposit on the HC anode, making the SEI thicker, increasing the interfacial impedance, and catalyzing the electrolyte reduction, thereby reducing the battery life. [35,36] To deeply understand this process, HC anodes from pouch batteries after 300 cycles at 3.8 V, 4.0 V and 4.2 V upper voltages were observed through SEM/EDS. There is Ni/Fe/Mn deposition on the HC anode, and spotted and mossy by-products are attached to the HC surface obviously degrading the HC structure (Fig. 5a-d and S39). The three types of HC anode further reassembled into Na||HC half battery for EIS measurements, the interfacial impedance of HC anode increases only slightly with the charging cut-off voltage increase. And the impedance of HC anode is much smaller than that of NFM cathode through the whole cycle, indicating the matter of NFM in full battery (Fig. S40-42). However, the interfacial impedance of HC anode increases significantly with long cycling (Fig. S43).

From the NFM cathode, the TM dissolution amount was quantitatively characterized by inductively coupled plasma-optical emission spectrometer (ICP-OES). Fresh NFM cathode was assembled into full batteries and charged to 3.8 V, 4.0 V and 4.2 V at 0.1 C severally, then extracted from batteries, washed with DMC, and dipped in the electrolytes that were tested by ICP-OES (Fig. 5f). From the test results, it is found that the Fe and Mn dissolution are more serious than Ni, which can be attributed to the ion migration probability increased by the Jahn-Teller distortion of Fe^{4+} and the high reaction activity of Mn^{4+} to soluble Mn^{2+} under the H^+ attack. [35, 37]Besides, with the charging cut-off voltage increase, the dissolution amount of total TM from NFM cathode increases.

Therefore, the TM dissolution, mitigation and deposition, indicate not only the degraded structure and blocked Na^+ migration in NFM cathode, but also the aggravated side reactions of electrolyte and damaged structure of SEI for HC anode. It is a chemical crosstalk between electrodes resulting in the structure-performance combined failure during cycling especially under high charging cut off voltage.

5. Case of high-voltage NFM performance improvement

Since NFM in full battery cycling at 4.2 V high upper voltage experiences serious particle cracking due to harmful X and O3' phase transition that cathode-electrolyte side reactions continuously happen and thick CEI forms on NFM particles, for a preliminary attempt boron-contained additives (lithium difluoro oxalate borate (LiDFOB) and trimethyl borate (TMB)) are introduced into the electrolyte aiming to form stable CEI and protect NFM cathode, thus suppressing the capacity degradation from active ion loss and active NFM loss at high-voltage. [38–43] The contrastive structure-performance relationships and improvement mechanism are presented in Fig. 6a. The additives can self-sacrifice oxidate on NFM during charge due to their high HOMO energy, [44] which can inhibit the carbonate solvent decomposition, promote more PF_6^- decomposition and adsorb by-products such as HF, thus forming

View Article Online
DOI: 10.1039/D5EB00077G

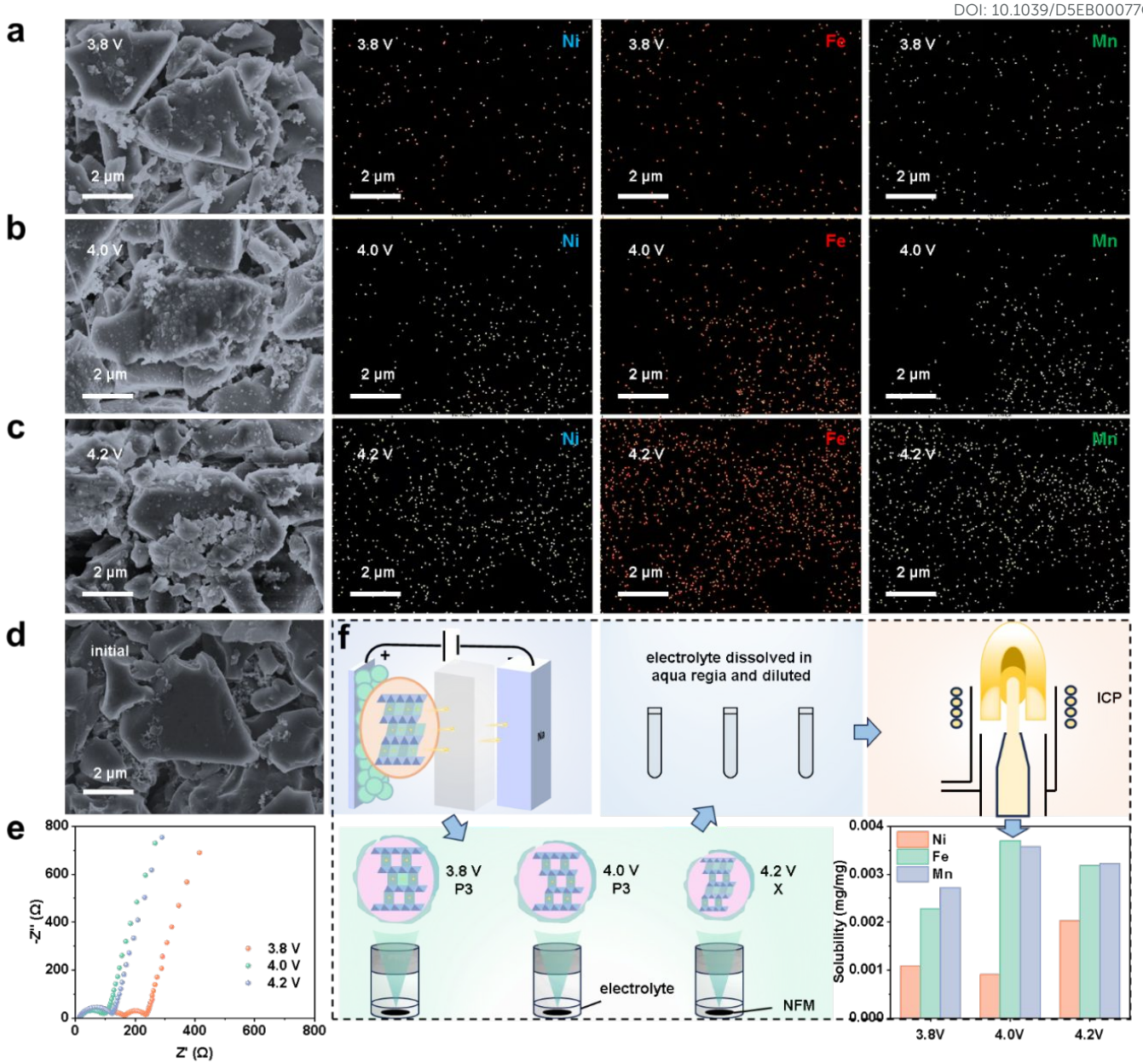

Fig. 5 TM ion dissolution, mitigation and deposition on HC anode. (a-c) SEM and elemental mapping images of anode from HC||NFM batteries cycled at 3.8 V, 4.0 V, and 4.2 V upper voltages respectively. (d) SEM image of initial anode. (e) Nyquist plots of Na||HC half batteries whose HC electrodes were from HC||NFM pouch batteries after 300 cycles at 3.8 V, 4.0 V and 4.2 V respectively. (f) ICP-OES testing process and results of TM dissolution in the electrolyte from NFM cathode charging to 3.8 V, 4.0 V, and 4.2 V (the unit: mg/mg means mg dissolved TM per mg NFM).

inorganic-rich CEI. The XPS spectra of the NFM cathode after cycling in the electrolyte with boron-contained additive demonstrate the achievement of this effect (Fig. 6b). The comprehensive electrochemical performance of NFM including high-voltage, high-temperature and fast charging cycling is greatly improved (Fig. 6c and S44-46). The interfacial impedance of NFM with the boron-contained additives are much smaller, indicating that the interface is indurative enough to suppress the interfacial parasitic reaction and exhibits high ion conductivity (Fig. S47). Besides, the structural stability of NFM is improved (Fig. S48-49). Therefore, the electrolytes with boron-contained additives supress the active ion loss and active cathode loss significantly, and can be a case improvement strategy addressing high-voltage failure of NFM cathode.

View Article Online
DOI: 10.1039/D5EB00077G

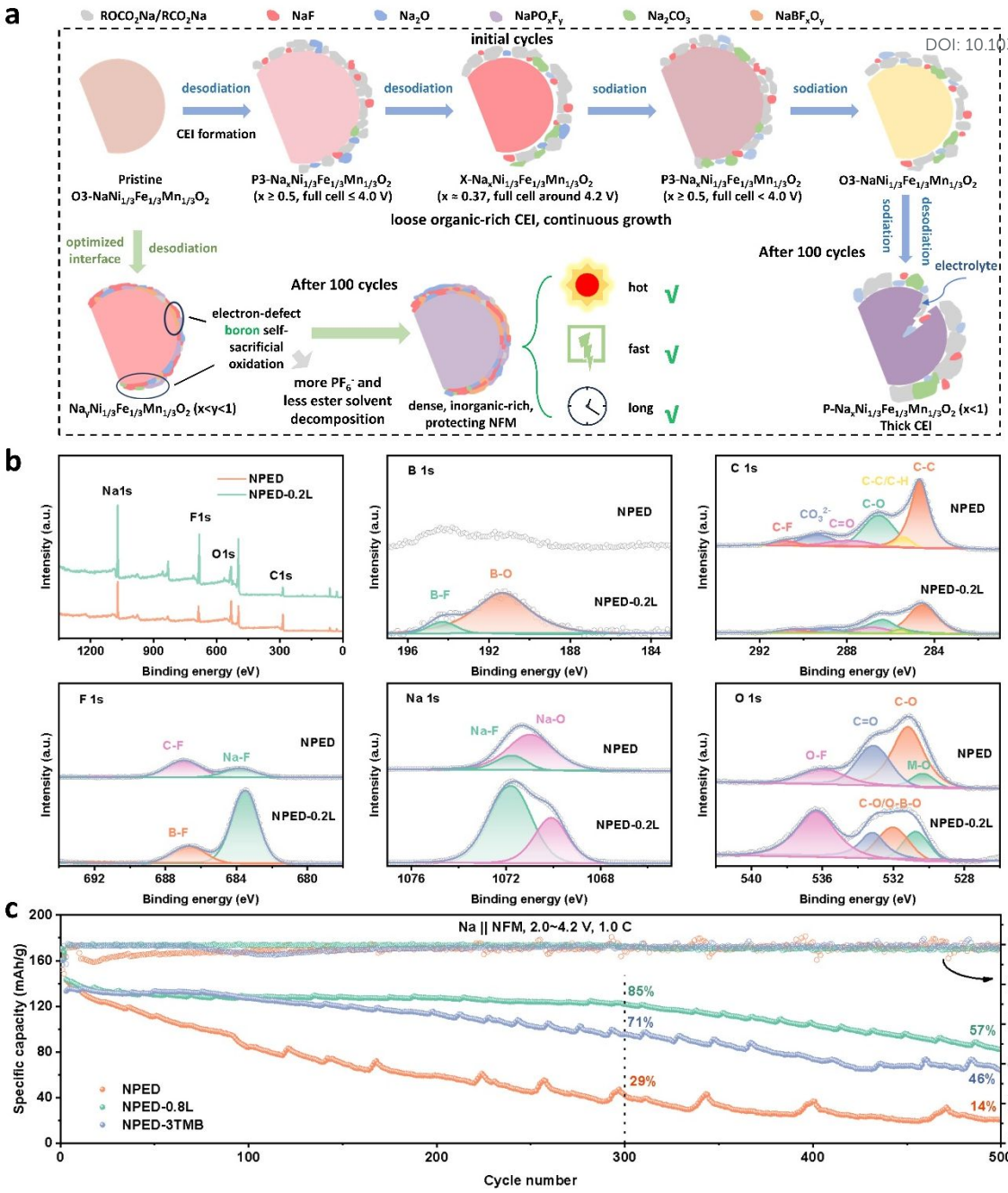

Fig. 6 (a) Schematic illustration of CEI growth on NFM particles during high-voltage cycling and reference case of a stable interface design. (b) Comparison of the XPS spectra of NFM in NPED and NPED-0.2L electrolytes after 500 cycles with the voltage range of 2.0~4.2 V at 60 °C. (c) Long cycling performance of Na||NFM in NPED, NPED-0.8L and NPED-3TMB electrolytes with the voltage range of 2.0~4.2 V at 1.0 C and room temperature. NPED: 1 M NaPF6 in EC/DEC. NPED-0.2L: 0.2 wt.% LiDFOB in NPED. NPED-0.8L: 0.8 wt.% LiDFOB in NPED. NPED-3TMB: 3 wt.% TMB in NPED.

Conclusions

This work reveals the high-voltage degradation mechanism of layered cathode-based SIBs by uncovering the capacity degradation sources through reverse coin half battery, tracing the structural evolution of the cathode through operando spectroscopy, and characterizing the material failure processes through XRD, electrochemical techniques and electron microscopy. At 4.0 V upper voltage, HC||NFM full battery can remain both high specific energy and long cycle life, benefiting from a reversible structural evolution of O3-P3-O3 phase sequence. At 4.2 V upper voltage, although this battery system has high energy density in early cycles, its cycling stability drops dramatically, with the capacity loss coming from the interfacial side reactions and the structural degradation of

cathode. During a cycle at this upper voltage, NFM experiences a complex irreversible structural evolution of O3-P3-X-O3'-P3-O3 phase sequence, with the unit cell expansion-contraction only during charging, exacerbating particle cracking and interfacial parasitic reactions. Meanwhile, the reaction kinetics is obviously retarded and the polarization gets larger more than twice. Finally, boron-contained additives were introduced for self-sacrificial oxidation on the NFM surface to form an inorganic-rich dense interface, thereby protecting NFM and obtaining excellent comprehensive electrochemical performance. This work provides a fundamental insight into the high-voltage failure mechanism of layered cathode-based SIBs, and a powerful reference to design long-life high-specific energy SIBs and stable high-voltage NFM cathode.

Experimental

Electron microscope

The morphology of materials was observed through scanning electron microscope (SEM). The type of SEM instrument is Hitachi TM3030 and Zeiss GeminiSEM 500. The working voltage of Hitachi TM3030 is 15 kV and that of Zeiss GeminiSEM 500 is 30 kV. The element mapping on material surface was achieved by energy dispersion spectrum (EDS) in Zeiss GeminiSEM 500. The bulk structure of materials and cathode-electrolyte interface (CEI) were observed through transmission electron microscope (TEM, JEOL JEM-2100plus) and the working voltage of TEM instrument is 200 Kv.

Operando and post-mortem XRD measurements

Operando XRD measurements were conducted to trace the structural evolution of NFM cathode in working pouch full cell on a Malvern PANalytical Empyrean diffractometer with Ag Kα radiation. The position was from 5.2 ° to 28.0 ° spending 17 min. Ex-situ XRD measurements were conducted to judge the material structure also on Malvern PANalytical Empyrean diffractometer with a scan rate of 10 ° min^{-1} and Cu Kα radiation.

Spectral characterizations

Raman spectroscopy (Horiba LabRAM HR Evolution) was used to characterize the structure of NFM and HC powders, with a 532 nm wavelength of laser and a 0.28 mW power. X-ray photoelectron spectroscopy (XPS, Thermo Scientific ESCALAB Xi+) was used to analyze the surface component of NFM cathode. The NFM cathode were taken out from cycled cells, dipped in dimethyl carbonate (DMC) solvent and dried enough to remove the residual electrolyte on NFM. Inductively coupled plasma-optical emission spectroscopy (ICP-OES, SPECTRO SPECTROBLUE FMX36) was used to identify the transition metal content dissolved from NFM cathode to the electrolyte. The fully charged NFM cathode of 3.8 V, 4.0 V and 4.2 V were dipped in electrolyte for 24 h respectively, and then taken out. Subsequently, the electrolytes were dissolved with aqua regia and diluted with ultrapure water for ICP-OES measurements.

Electrochemical measurements

Na||NFM and Na||HC half cells were assembled to evaluate their electrochemical performance including capacity, cycling stability, rate performance, electrochemical impedance spectrum (EIS) and galvanostatic intermittent titration (GITT). After assembled, coin cells were hold for 6 hours before testing. The cathode electrode was fabricated with 80 wt.% NFM, 10 wt.% PVDF and 10 wt.% Super P carbon conductive agent, N-methyl-1,2-pyrrolidone (NMP) as the solvent and dried at 80 °C for 12 h, for cycling and cyclic voltammetry tests. Porous glass fiber separator (Whatman, GF/D) was used in coin cell (CR2016) to well hold the electrolyte in long cycling and 0.1 C corresponds to 13 mA/g current density. EIS measurements were performed on Solartron electrochemical workstation and the voltage amplitude was 10 mV with the frequency range from 10^5 Hz to 0.1 Hz. GITT tests were conducted on Land battery tester with the voltage range from 2.0 V to each selected upper voltage.

Author contributions

Shini Lin and Wei Li conceived the idea and collaborated to complete all experiments, tests and write. Conceptualization: Shini Lin and Wei Li. Experimental design and investigation: Shini Lin. Data analysis: Shini Lin, Wei Li, Huiya Yang, Minghui Chen, Jing Zeng and Peng Zhang. Validation: Shini Lin, Yuan Qin and Honghao Xie. Writing – original draft: Shini Lin. Writing – review & editing: Shini Lin, Wei Li, Peng Zhang and Jinbao Zhao. Funding acquisition & resources: Jinbao Zhao.

Conflicts of interest

There are no conflicts to declare.

Data availability

The authors confirm that the findings of this study are available within the main text and SI.

Acknowledgements

The authors gratefully acknowledge financial support from the National Key Research and Development Program of China [2021YFB2400300], Yunnan Natural Science Foundation Project [202202AG050003] and National Natural Science Foundation of China [22021001]. And we are grateful to Tan Kah Kee Innovation Laboratory (IKKEM) for help with TEM and ICP measurements.

References

1 Y. Gao, H. Zhang, J. Peng, L. Li, Y. Xiao, L. Li, Y. Liu, Y. Qiao and S.-L. Chou, *Carbon Energy*, 2024, **6**, e464.
2 C. Vaalma, D. Buchholz, M. Weil and S. Passerini, *Nat Rev Mater*, 2018, **3**, 1–11.
3 J.-Y. Hwang, S.-T. Myung and Y.-K. Sun, *Chem. Soc. Rev.*, 2017, **46**, 3529–3614.
4 H. S. Hirsh, Y. Li, D. H. S. Tan, M. Zhang, E. Zhao and Y. S. Meng, *Advanced Energy Materials*, 2020, **10**, 2070134.

5 D. Hou, D. Xia, E. Gabriel, J. A. Russell, K. Graff, Y. Ren, C.-J. Sun, F. Lin, Y. Liu and H. Xiong, *ACS Energy Lett.*, 2021, **6**, 4023–4054.
6 J. Liu, Y. Zhang, J. Zhou, Z. Wang, P. Zhu, Y. Cao, Y. Zheng, X. Zhou, C. Yan and T. Qian, *Advanced Functional Materials*, 2023, **33**, 2302055.
7 G. Liu, W. Wan, Q. Nie, C. Zhang, X. Chen, W. Lin, X. Wei, Y. Huang, J. Li and C. Wang, *Energy Environ. Sci.*, 2024, **17**, 1163–1174.
8 G. Bree, D. Horstman and C. T. J. Low, *Journal of Energy Storage*, 2023, **68**, 107852.
9 H. Jo, J. H. Park, D. Choi, K. Kim and S. An, *Advanced Materials*, **n/a**, 2407719.
10 Y.-J. Guo, R.-X. Jin, M. Fan, W.-P. Wang, S. Xin, L.-J. Wan and Y.-G. Guo, *Chem. Soc. Rev.*, 2024, **53**, 7828–7874.
11 G.-L. Xu, R. Amine, Y.-F. Xu, J. Liu, J. Gim, T. Ma, Y. Ren, C.-J. Sun, Y. Liu, X. Zhang, S. M. Heald, A. Solhy, I. Saadoune, W. L. Mattis, S.-G. Sun, Z. Chen and K. Amine, *Energy Environ. Sci.*, 2017, **10**, 1677–1693.
12 X. Liang, J.-Y. Hwang and Y.-K. Sun, *Advanced Energy Materials*, 2023, **13**, 2301975.
13 R. Dong, L. Zheng, Y. Bai, Q. Ni, Y. Li, F. Wu, H. Ren and C. Wu, *Advanced Materials*, 2021, **33**, 2008810.
14 S. Qiu, L. Xiao, M. L. Sushko, K. S. Han, Y. Shao, M. Yan, X. Liang, L. Mai, J. Feng, Y. Cao, X. Ai, H. Yang and J. Liu, *Advanced Energy Materials*, 2017, **7**, 1700403.
15 Z. Wang, X. Feng, Y. Bai, H. Yang, R. Dong, X. Wang, H. Xu, Q. Wang, H. Li, H. Gao and C. Wu, *Advanced Energy Materials*, 2021, **11**, 2003854.
16 T. Perveen, M. Siddiq, N. Shahzad, R. Ihsan, A. Ahmad and M. I. Shahzad, *Renewable and Sustainable Energy Reviews*, 2020, **119**, 109549.
17 N. LeGe, X.-X. He, Y.-X. Wang, Y. Lei, Y.-X. Yang, J.-T. Xu, M. Liu, X. Wu, W.-H. Lai and S.-L. Chou, *Energy Environ. Sci.*, 2023, **16**, 5688–5720.
18 Y. Li, A. Vasileiadis, Q. Zhou, Y. Lu, Q. Meng, Y. Li, P. Ombrini, J. Zhao, Z. Chen, Y. Niu, X. Qi, F. Xie, R. Van Der Jagt, S. Ganapathy, M.-M. Titirici, H. Li, L. Chen, M. Wagemaker and Y.-S. Hu, *Nat Energy*, 2024, **9**, 134–142.
19 H. Yang, D. Wang, Y. Liu, Y. Liu, B. Zhong, Y. Song, Q. Kong, Z. Wu and X. Guo, *Energy Environ. Sci.*, 2024, **17**, 1756–1780.
20 L. Chen, X. Fan, E. Hu, X. Ji, J. Chen, S. Hou, T. Deng, J. Li, D. Su, X. Yang and C. Wang, *Chem*, 2019, **5**, 896–912.
21 Y. Zhao, Q. Liu, X. Zhao, D. Mu, G. Tan, L. Li, R. Chen and F. Wu, *Materials Today*, 2023, **62**, 271–295.
22 S. Feng, C. Zheng, Z. Song, X. Wu, M. Wu, F. Xu and Z. Wen, *Chemical Engineering Journal*, 2023, **475**, 146090.
23 Y. You, S. Xin, H. Y. Asl, W. Li, P.-F. Wang, Y.-G. Guo and A. Manthiram, *Chem*, 2018, **4**, 2124–2139.
24 K. Zhang, Z. Xu, G. Li, R.-J. Luo, C. Ma, Y. Wang, Y.-N. Zhou and Y. Xia, *Advanced Energy Materials*, 2023, **13**, 2302793.
25 T.-Y. Yu, J. Kim, G. Oh, M. H. Alfaruqi, J.-Y. Hwang and Y.-K. Sun, *Energy Storage Materials*, 2023, **61**, 102908.
26 M. Keller, D. Buchholz and S. Passerini, *Advanced Energy Materials*, 2016, **6**, 1501555.
27 Y. Yu, D. Ning, Q. Li, A. Franz, L. Zheng, N. Zhang, G. Ren, G. Schumacher and X. Liu, *Energy Storage Materials*, 2021, **38**, 130–140.
28 N. Li, J. Ren, R. Dang, K. Wu, Y. L. Lee, Z. Hu and X. Xiao, *Journal of Power Sources*, 2019, **429**, 38–45.
29 Y. Li, F. Wu, Y. Li, M. Liu, X. Feng, Y. Bai and C. Wu, *Chem. Soc. Rev.*, 2022, **51**, 4484–4536.
30 T.-Y. Yu, J. Kim, G. Oh, M. H. Alfaruqi, J.-Y. Hwang and Y.-K. Sun, *Energy Storage Materials*, 2023, **61**, 102908.
31 K. Zhang, Z. Xu, G. Li, R.-J. Luo, C. Ma, Y. Wang, Y.-N. Zhou and Y. Xia, *Advanced Energy Materials*, 2023, **13**, 2302793.
32 X. Liu, Y. Wan, M. Jia, H. Zhang, W. Xie, H. Hu, X. Yan and X. Zhang, *Energy Storage Materials*, 2024, **67**, 103313.
33 X. Zeng, G.-L. Xu, Y. Li, X. Luo, F. Maglia, C. Bauer, S. F. Lux, O. Paschos, S.-J. Kim, P. Lamp, J. Lu, K. Amine and Z. Chen, *ACS Appl. Mater. Interfaces*, 2016, **8**, 3446–3451.
34 S. Komaba, N. Yabuuchi, T. Nakayama, A. Ogata, T. Ishikawa and I. Nakai, *Inorg Chem*, 2012, **51**, 6211–6220.
35 S. Chu and S. Guo, *Advanced Functional Materials*, 2024, **34**, 2313234.
36 Y. Liu, Y.-H. Zhang, J. Ma, J. Zhao, X. Li and G. Cui, *Chemistry of Materials*, DOI:10.1021/acs.chemmater.3c02115.
37 M. Jeong, H. Lee, J. Yoon and W.-S. Yoon, *Journal of Power Sources*, 2019, **439**, 227064.
38 K. Ma, Y. Cao, S. Zhang, Y. Zhang, S. Fang, X. Han, F. Jin and J. Sun, *Nano Lett.*, 2024, **24**, 8826–8833.
39 Z. Liu, W. Hou, H. Tian, Q. Qiu, I. Ullah, S. Qiu, W. Sun, Q. Yu, J. Yuan, L. Xia and X. Wu, *Angewandte Chemie International Edition*, 2024, **63**, e202400110.
40 J. Li, J. Yang, Z. Ji, M. Su, H. Li, Y. Wu, X. Su and Z. Zhang, *Advanced Energy Materials*, 2023, **13**, 2301422.
41 S. Li, H. Xu, Y. Zhu, Z. Yang, Y. Bao and Y. Chen, *J. Mater. Chem. A*, 2024, **12**, 31347–31361.
42 J. Liu, X. Li, J. Huang, G. Yang and J. Ma, *Advanced Functional Materials*, 2024, **34**, 2312762.
43 Q. Liu, G. Yang, S. Liu, M. Han, Z. Wang and L. Chen, *ACS Appl. Mater. Interfaces*, 2019, **11**, 17435–17443.
44 Y. Zhang, Y. Chen, Q. He, J. Ke, W. Wang, J.-F. Wu, P. Gao, Y. Li and J. Liu, *Journal of Energy Chemistry*, 2024, **92**, 639–647.

View Article Online
DOI: 10.1039/D5EB00077G

Data availability

The authors confirm that the findings of this study are available within the main text and SI.